Pharm Res (2010) 27:2624–2632
DOI 10.1007/s11095-010-0259-7

RESEARCH PAPER

Structural Interpretation in Composite Systems Using Powder X-ray Diffraction: Applications of Error Propagation to the Pair Distribution Function

Michael D. Moore • Zhenqi Shi • Peter L. D. Wildfong

Received: 15 June 2010 / Accepted: 21 August 2010 / Published online: 2 September 2010

ABSTRACT

Purpose To develop a method for drawing statistical inferences from differences between multiple experimental pair distribution function (PDF) transforms of powder X-ray diffraction (PXRD) data.

Methods The appropriate treatment of initial PXRD error estimates using traditional error propagation algorithms was tested using Monte Carlo simulations on amorphous ketoconazole. An amorphous felodipine:polyvinyl pyrrolidone:vinyl acetate (PVPva) physical mixture was prepared to define an error threshold. Co-solidified products of felodipine:PVPva and terfenadine:PVPva were prepared using a melt-quench method and subsequently analyzed using PXRD and PDF. Differential scanning calorimetry (DSC) was used as an additional characterization method.

Results The appropriate manipulation of initial PXRD error estimates through the PDF transform were confirmed using the Monte Carlo simulations for amorphous ketoconazole. The felodipine:PVPva physical mixture PDF analysis determined $\pm 3\sigma$ to be an appropriate error threshold. Using the PDF and error propagation principles, the felodipine:PVPva co-solidified product was determined to be completely miscible, and the terfenadine:PVPva co-solidified product, although having appearances of an amorphous molecular solid dispersion by DSC, was determined to be phase-separated.

Conclusions Statistically based inferences were successfully drawn from PDF transforms of PXRD patterns obtained from composite systems. The principles applied herein may be universally adapted to many different systems and provide a fundamentally sound basis for drawing structural conclusions from PDF studies.

KEY WORDS amorphous dispersion · error propagation · Monte Carlo simulation · PDF· PXRD

ABBREVIATIONS

DSC	differential scanning calorimetry
PDF	pair distribution function
PVPva	polyvinyl pyrrolidone:vinyl acetate copolymer
PXRD	powder X-ray diffraction
G	pair distribution function
r	inter-atomic radial distance
ρ	local number density
ρ_0	average number density
Q	scattering vector magnitude
S	structure function
σ	standard error
T_g	glass transition temperature
h_0	statistical null hypothesis
h_A	statistical alternative hypothesis
R	sum-of-squares difference agreement factor

INTRODUCTION

Advanced analytical techniques used to characterize pharmaceutically relevant materials properties are becoming increasingly sensitive to changes in short-range order of material structure. At the forefront of these advancements is a total scattering powder X-ray diffraction (PXRD) method

M. D. Moore · Z. Shi · P. L. D. Wildfong (✉)
Duquesne University
Graduate School of Pharmaceutical Sciences
600 Forbes Ave.
Pittsburgh, Pennsylvania 15282, USA
e-mail: wildfongp@duq.edu

adapted from the inorganic materials science literature, commonly referred to as the atomic pair distribution function (PDF). The PDF transform exploits the Fourier relationship between powder diffraction intensity and the real space arrangement of atomic species. It has been used extensively to study crystalline, nanocrystalline, and amorphous inorganic materials, and its application in the pharmaceutical literature has increased substantially in the last decade.

Recent applications of the PDF in the pharmaceutical literature include the investigation of dehydration mechanisms in excipients (1), phase differentiation (2,3), assessment of structural changes during pharmaceutical manufacturing (4,5), and characterization of solid dispersions (6–8). Given the wealth of knowledge available from the PDF transform, PDFs are subject to errors in interpretation, provided consideration of experimental uncertainty is neglected. Additionally, errors made to pre-Fourier transformed intensities manifest as pattern anomalies oftentimes mistaken for structural phenomena, thereby further detracting from the merit of the study. Deriving an error estimate for a PDF pattern would largely increase the value of PDF-related conclusions.

An appropriate estimate of error at the outset of the experiment and subsequent propagation through the entire mathematical transformation would significantly aid in drawing meaningful conclusions from PDF studies. Experimental errors in the PXRD experiment may arise from quantum counting inefficiencies, experimental imprecision, sample inhomogeneities, *etc.* and should be propagated and accounted for when interpreting PDFs. In addition to uncertainties in the PXRD experiment, the lack of infinite momentum transfer resolution, as well as inaccurate data corrections applied to intensity data, affect the degree of uncertainty in the resulting PDF. The inherent artifacts incurred as a result of Fourier transforming lower energy X-ray source data to real-space representation are well known, and when treated appropriately (9) are less significant contributors to errors in the PDF.

Error propagation methods to assess the fit between a theoretical PDF calculated from a known crystal structure and experimental PDF have been developed and applied in the materials sciences literature (10,11). As it is becoming routine to compare two experimentally derived PDFs (*i.e.* two individual components versus composite materials), a question arises as to appropriate treatment of each individual error source in combined comparisons. In this study, the propagation of initial PXRD error estimates through the PDF transform is presented. Monte Carlo simulations were performed to assess the validity of applying traditional error propagation algorithms to accurately estimate uncertainty in the resulting PDF. The propagated error estimates for individual experimentally derived PDFs were mathematically combined to define uncertainty intervals around difference plots. Statistical hypothesis inferences were drawn from these intervals to aid in identifying differences between experimental PDF patterns attributable to structure as opposed to those resulting from random error. The aforementioned principles were applied to co-solidified products in an attempt to assess drug: excipient miscibility, an area where differentiation between structural information and error in the PDF is of the utmost importance.

MATERIALS AND METHODS

Materials

Ketoconazole was purchased from Spectrum Chemicals (New Brunswick, NJ), polyvinyl pyrrolidone:vinyl acetate (PVPva) was purchased from BASF (Ludwigshafen, Germany), terfenadine was purchased from Sigma-Aldrich (St. Louis, MO) and felodipine was purchased from Tecoland (Edison, NJ). Molecular structures for the compounds used in this study are shown in Fig. 1.

Solid Dispersion Preparation

Co-solidified products were prepared using the melt-quench method (12). Briefly, the powdered components were physically mixed in a scintillation vial and added to a crucible heated in a silicone oil bath at a temperature sufficient to melt the mixture. The molten mixture was held isothermally for 30 min. The crucible containing the molten mixture was then quenched in an ice water bath. Individual amorphous phases were produced by holding the sample above the melting temperature in a crucible for 10 minutes followed by quenching in an ice bath. All samples were removed from the bottom of the crucible intact for analysis.

Powder X-ray Diffraction (PXRD)

The PXRD data were collected in transmission geometry using an X'Pert Pro MPD system (PANalytical B.V., Almelo, the Netherlands) equipped with a copper anode ($\lambda = 1.5406$ Å), an auxiliary elliptical mirror, and an X'Celerator™ detector. The operational voltage and amperage were set to 45.0 kV and 40.0 mA, respectively. Diffraction patterns were acquired on intact samples, sandwiched between two layers of Kapton® film and subsequently placed on a spinning vertical sample stage (16 rpm). Experimental parameters include an irradiation time of 51.04 sec per step and an angular step size of 0.02° 2θ over a 2–100° 2θ range.

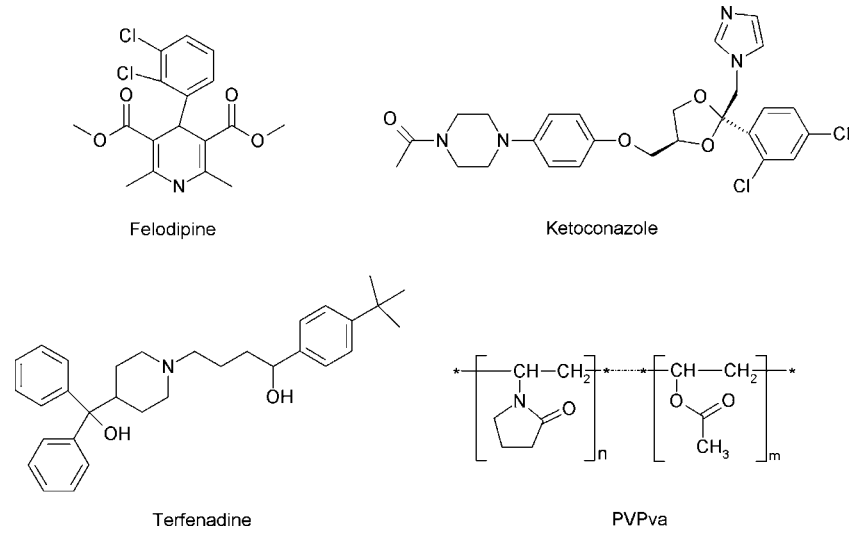

Fig. 1 Molecular structures for felodipine, ketoconazole, terfenadine, and PVPva.

Differential Scanning Calorimetry (DSC)

Glass transition temperatures (T_g) were measured using a Q100 DSC (TA Instruments, New Castle, DE) under constant nitrogen purge (~50 mL/min). A three-point enthalpy and temperature calibration was performed at 20°C/min using o-terphenyl, indium, and tin standards. In an attempt to avoid artifacts arising from grinding samples, approximately 5 mg intact "sample chips" were hermetically sealed in aluminum pans. To normalize thermal history, samples were first heated at 20°C/min to 105°C, held isothermally for 2 min, and subsequently cooled to −20°C at 20°C/min. Samples were then cycled through T_g at 20°C/min for temperature determination. Ideal glass transition temperatures for drug:polymer amorphous molecular solid dispersions were calculated using the Couchman-Karasz equation (13) and are listed in Table I.

Pair Distribution Function (PDF)

The PDF is a total scattering method that exploits the Fourier relationship between X-ray diffraction intensity and the real-space arrangement of atoms, given appropriate data treatment (14,15). This method has received extensive attention in the inorganic literature with an increasing number of pharmaceutical applications reported recently (1–3,6,8). The PDF, *G(r)*, is defined as

$$G(r) = 4\pi r[\rho(r) - \rho_o] \quad (1)$$

where $\rho(r)$ and ρ_o are the local and average atomic number densities, respectively, and r is the inter-atomic separation distance. The PDF calculates the probability of finding atom pairs separated by a distance r, and is obtained by Fourier transform of the reciprocal space structure function, *S(Q)*, according to

$$G(r) = \frac{2}{\pi}\int_0^{Q\,\max} Q[S(Q) - 1]\sin(Qr)dQ \quad (2)$$

where *S(Q)* is the structure factor obtained from a diffraction experiment and Q is the magnitude of the scattering vector. The term Q_{max} is the momentum transfer resolution of the diffraction experiment, which is dependent on the wavelength of radiation used and the maximum diffraction angle (°2θ) of data collection. Corrections consistent with those outlined by Egami and Billinge (14) were made to the measured diffraction data leading, to the calculation of the structure function. All intensity corrections (*e.g.* background due to Kapton® film scattering, absorption, *etc.*) and PDF calculations were performed using software developed in-house in the Matlab programming environ-

Table I DSC and PDF Results

	DSC analysis		PDF analysis			
	Ideal T_g (°C)	T_g (°C)	*R* value	Drug conc. (w/w)	Polymer conc. (w/w)	Conclusion
Felodipine:PVPva	62.1	66.9 (0.015)	0.2126	0.81	0.19	miscible
Terfenadine:PVPva	77.48	60.7 (0.21)	0.0864	0.73	0.27	phase-separated

ment (v7.1, MathWorks, Natick, MA) based on published equations. The PDF transforms were optimized using the G_{low} quality criteria introduced by Peterson *et al.* (9).

Error Propagation

The method of error propagation through the PDF transform has been derived and applied in previous work (11,14). If it is assumed that the measurement of each individual observation is statistically independent of all others (*i.e.* the count intensity at a given diffraction angle is independent of all others), the covariance between observations is eliminated. It is worthwhile to note that the aforementioned assumption is appropriate in PXRD experiments, provided the mathematical manipulations to the raw diffraction pattern do not introduce statistical correlation among individual data points (*i.e.* windowed smoothing, interpolation). When a quantity T is the sum of two independent observations, X_1 and X_2, each having their own error estimate, $\sigma(X_1)$ and $\sigma(X_2)$, the estimated error $\sigma(T)$ is

$$\sigma(T) = \sqrt{(\sigma(X_1))^2 + (\sigma(X_2))^2} \tag{3}$$

The quantity T calculated from the product of a constant value, c, and X has an estimated error given by

$$\sigma(T) = c \bullet \sigma(X) \tag{4}$$

When a quantity T is the product of two independent observations, X_1 and X_2, each having their own error estimate, $\sigma(X_1)$ and $\sigma(X_2)$, the estimated error $\sigma(T)$ is

$$\frac{\sigma(T)}{T} = \frac{\sigma(X_1)}{X_1} + \frac{\sigma(X_2)}{X_2} \tag{5}$$

Error propagation was performed by setting up two data vectors. The first data vector contained the raw PXRD intensity values for a given powder pattern. The second vector contained the initial error estimates for each intensity value. The vectors were propagated side-by-side through to the calculation of the structure function using the principles outlined in Eqs. 3, 4, and 5 for the mathematical manipulations to the error vector.

The final step of the PDF method involves the sine Fourier transform of the structure function, $S(Q)$, into real-space representation. Given accurate propagation of error up through calculation of the structure factor and no introduction of statistical correlation among the independent scattering events, a good estimate of the standard uncertainty in the PDF, $\sigma(G(r))$, is given by

$$\sigma\left(G\left(r_j\right)\right) = \sqrt{\frac{4}{\pi^2}\sum_i \left(Q_i \sin\left(Q_i r_j\right)\Delta Q_i\right)^2 \sigma(S(Q_i))^2} \tag{6}$$

where $\sigma(S(Q))$ is the error estimate of the structure function.

Monte Carlo Simulation

Monte Carlo refers to a broad class of methods that employ generation of random numbers as a starting point for solving a complicated numerical problem. Monte Carlo methods are often used to simulate physical and mathematical systems. They are especially useful for modeling phenomena having significant uncertainty. The simulation typically begins with defining a distribution of possible inputs. An input generated from the distribution is used to perform deterministic computations to obtain an individual result. Finally, the results from individual computations are compiled and interpreted (16).

The raw PXRD counts go through a number of mathematical manipulations when transformed using the PDF algorithm, oftentimes optimized according to specific quality criteria (9). In order to confirm the appropriate propagation of an initial raw count error estimate, Monte Carlo simulations were employed. The simulations began with a defined distribution of intensity values at each °2θ. The distribution at each specific scattering angle (°2θ) was formed by using the raw intensity (*i.e.* counts) as the distribution mean and the error estimate as the spread. Simulated PXRD patterns were formed by randomly selecting an intensity value from the previously defined distributions at each °2θ angle. Each simulated PXRD pattern was subsequently transformed into real-space representation using the PDF. After ten-thousand iterations, a matrix of PDF patterns spanning the variance of the simulated PXRD patterns was formed. The minimum and maximum $G(r)$ at each r-value in the PDF were compared to the error vector calculated using the previously defined equations.

RESULTS

The count of scattered intensity within a given time interval obtained from the PXRD experiment is subject to an unavoidable, random uncertainty due to statistical variation in quantum counting (17). This stochastic variation best follows a Poisson probability density function. Assuming that n counts occur in a specific time interval, the distribution possesses a mean and variance equal to n, when n is a positive integer (14). The standard deviation for n counts at the scattering angle $x°$ 2θ is, therefore, equal to the square-root of n and will serve as the initial error estimate.

Figure 2a shows the diffraction pattern for amorphous ketoconazole (black, solid line) and ±3 standard deviations

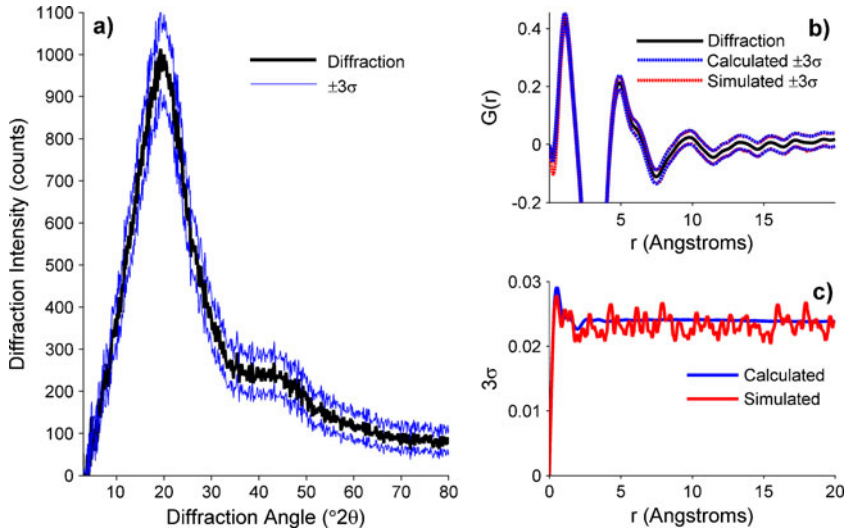

Fig. 2 **a** The diffraction pattern for amorphous ketoconazole (black, thick line) and ±3σ (blue, thin line); **b** the PDF transform of (a) (black, thick line), calculated ±3σ (blue, dashed line), and simulated ±3σ (red, dashed line); **c** absolute representation of calculated 3σ (blue) and simulated 3σ (red).

(blue, solid line). The subsequent PDF transform of the PXRD pattern is shown in Fig. 2b (zoomed, black, solid line). To confirm the appropriate propagation of error through the transform, Monte Carlo simulations were performed as previously described. The calculated error (blue, dashed lines) and simulated error (red, dashed lines) are shown as intervals in Fig. 2b and as absolute error values in Fig. 2c.

It is common practice to compare an experimentally obtained PDF to one calculated from a structural model. Previous studies have illustrated the advantages of error propagation to this particular application, but fail to specifically address comparisons between multiple experimental PDFs. Difference plots with error intervals calculated from experimental PDFs may assist in delineating random errors from true, structural variations. Figure 3a shows the PDF transform of a 50 wt% physical mixture of amorphous felodipine and PVPva (black, solid line) with an overlay of a linear combination of PDFs from amorphous felodipine and PVPva (blue, line with circles). Figure 3b shows the difference plot (black, solid line) obtained from the two traces in Fig. 3a. Additionally, the estimated combined error contribution (±3σ) calculated from the propagation through each transform is also shown as an interval around the difference (red, dashed lines), that is to say, an interval calculated from the combination of the two amorphous component PDFs comprising the blue trace and the physical mixture PDF represented by the black trace.

To illustrate the potential to differentiate random error from true structural differences, the error propagation principles were applied to the method outlined by Newman *et al.* (6) that was proposed to identify miscibility between a drug and excipient. Briefly, the PDF of a co-solidified product is compared to the linear combination of the PDFs obtained from the amorphous components comprising the mixture. The scaling constants for each individual component PDF serve as estimates for concentration of each amorphous phase in the co-solidified mixture, when the two components are not completely miscible. If the linear combination of the PDF for each amorphous component describes the PDF of the co-solidified sample, it is reasonable to conclude that the system is at least partially phase-separated as the short-range order (*i.e.* the static local structure) of the co-solidified product

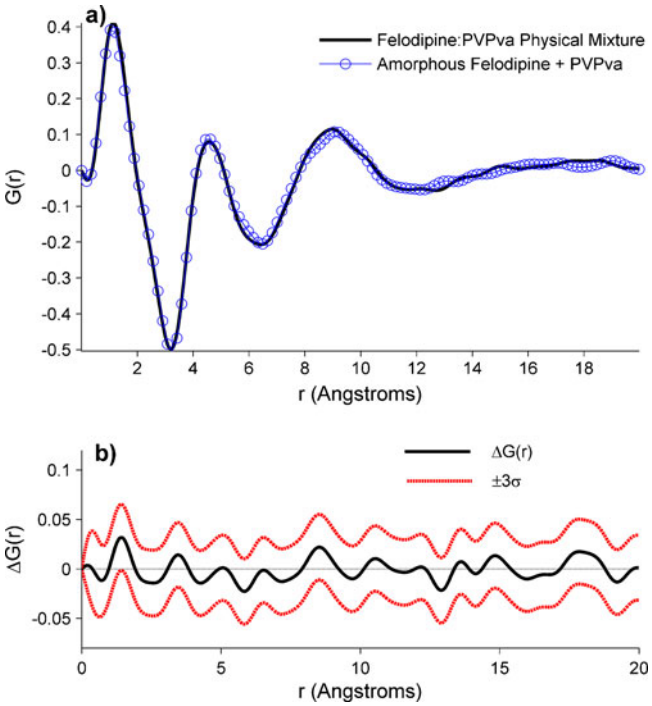

Fig. 3 **a** The PDF of a 50 wt% physical mixture of amorphous felodipine and PVPva (black) and the refined linear combination of the amorphous component PDFs (blue, circles); **b** the difference between the PDFs (black) and ±3σ (red, dashed line).

can be described by the intrinsic distances found in the amorphous API and polymer. Substantial differences between the PDF calculated from linear combination of the individual amorphous component PDFs and the PDF of the co-solidified sample are indicative of short-range order not presented in the individual components, (*i.e.* that of a unique packing pattern).

It is important to define miscibility in the context of amorphous molecular solid dispersions as opposed to the traditional use in thermodynamic solutions. Complete miscibility between a drug and polymer produces an overall physically stable amorphous phase. Rather than an equilibrium relationship, miscible systems may be described as a supersaturated phase, where the combined components collectively influence the resulting solid structure and intrinsic properties (*i.e.* molecular mobility and recrystallization tendency) associated with the newly formed short-range order.

Figure 4a shows the PDF transform (black, solid line) for a 75 wt% felodipine and PVPva co-solidified product. The superimposed trace (blue, circles and line) is the best refined linear combination of the amorphous component PDFs. Figure 4b shows the difference between the two PDFs (black, solid line) with the calculated ±3σ error estimates. As a point of comparison, Fig. 5a contains the PDF (black, solid line) for a 75 wt% terfenadine and PVPva co-solidified product. Superimposed is the best refined linear combination of the amorphous component PDFs. Figure 5b shows the difference between the two PDF traces (black, solid line) with the calculated ±3σ error estimates. The T_g for the co-solidified products in Figs. 4 and 5 are shown in Figs. 6 and 7, respectively. In both products, a single T_g event is observed (middle traces in Figs. 6 and 7) intermediate to the T_g observed for the pure components (top and bottom traces in Figs. 6 and 7). Table I summarizes the DSC and PDF results.

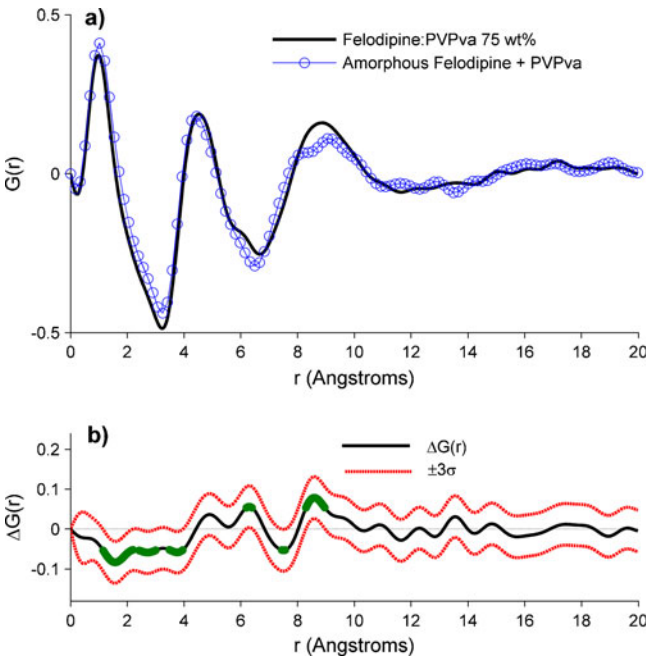

Fig. 4 **a** The PDF of a 75 wt% co-solidified product of felodipine and PVPva (black) and the refined linear combination of the amorphous component PDFs (blue, circles); **b** the difference between the PDFs (black) and ±3σ (red, dashed line), where the green dots are indicative of the error interval not containing zero.

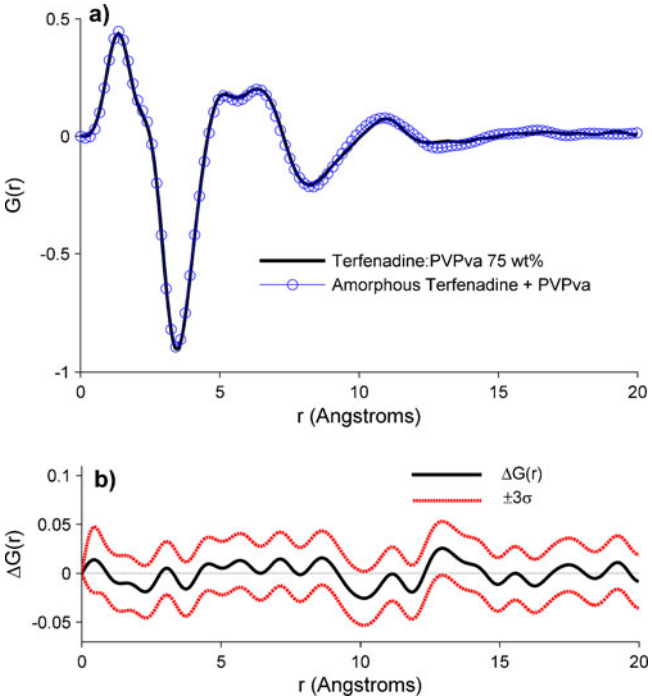

Fig. 5 **a** The PDF of a 75 wt% co-solidified product of terfenadine and PVPva (black) and the refined linear combination of the amorphous component PDFs (blue, circles); **b** the difference between the PDFs (black) and ±3σ (red, dashed line).

DISCUSSION

The PXRD experiment is traditionally regarded as robust. Fluctuations in scattering intensity attributable to experimental geometry (Lorentz factor) and radiation polarization are assumed to be insignificant contributors to the overall variance due to their precision (17,18). The uncertainty due to statistical variation in quantum counting, therefore, serves as an appropriate initial error estimate (Fig. 2a). Although this estimate does not contain all possible sources of error, it does enable the ability to rule out PDF differences that are small enough to be ruled out as significant.

By randomly selecting scattering intensities spanning the defined error interval for each scattering angle (°2θ) over ten-thousand iterations, the Monte Carlo simulation creates

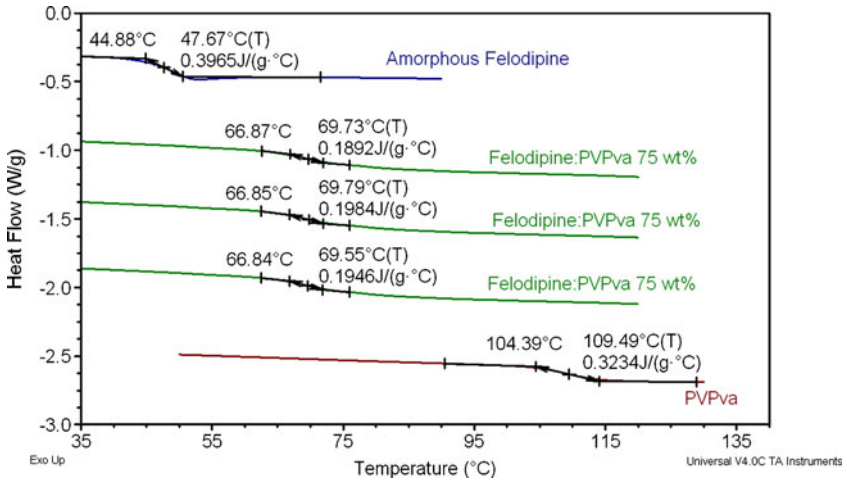

Fig. 6 The DSC thermograms for felodipine:PVPva systems (as labeled).

a matrix of diffraction patterns that possess the overall variance contained within the initial uncertainty estimate. The simulated patterns were individually transformed using the PDF algorithm. Since the simulated PXRD patterns span the total variance of the estimated uncertainty in reciprocal space, the resulting PDF patterns span that same variance in real-space. The propagated PDF uncertainty interval (Fig. 2b, blue, dashed lines) is in good agreement with the simulated PDF uncertainty interval (Fig. 2b, red, dashed lines). For a point of reference, the absolute PDF errors derived from propagation and simulation are given in Fig. 2c. The agreement between simulated and propagated errors confirms the appropriate propagation of the initial error estimate through the PDF transform.

Similar to comparing an experimental PDF to a calculated PDF from a structural model, the premise in these analyses is to identify correlations between PDFs while maintaining the ability to differentiate pattern dissimilarities attributable to structural differences from those attributable to random error. To do this, it is proposed that error intervals are estimated for the difference plot calculated between experimental PDFs of interest. In the difference between the calculated felodipine:PVPva PDF and the physical mixture PDF given in Fig. 3b (black, solid line), the uncertainty interval, obtained from the combined propagated error of the two PDF patterns, is shown to contain zero for every value of r. The PDF transform of a PXRD pattern of an amorphous felodipine:PVPva physical mixture would be expected to be the same as a linear combination of a PDF transform of a PXRD pattern of pure amorphous felodipine and a PDF transformed of a PXRD pattern of pure PVPva. This expectation is founded on the principle that a physical mixture of two amorphous materials would not alter the short-range order intrinsic to the two materials comprising the blend.

A null hypothesis may be formed stating that the difference between the two PDFs is equal to zero ($h_o : \mu_a - \mu_b = 0$). The alternative to the null hypothesis states the difference between the two PDFs is not equal to zero ($h_A : \mu_a - \mu_b \neq 0$). If, at any value of r, the $\pm 3\sigma$

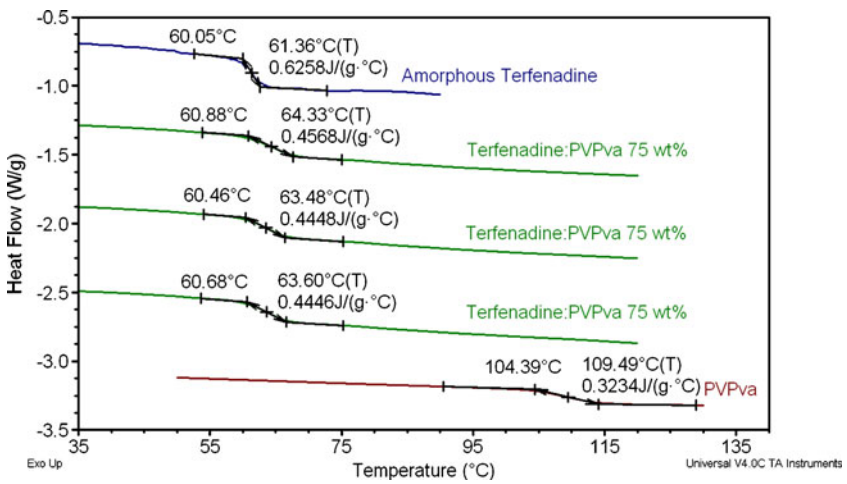

Fig. 7 The DSC thermograms for terfenadine:PVPva systems (as labeled).

interval around the difference plot contains zero, then the null hypothesis is accepted, as the difference between the two PDFs is statistically equivalent to zero. If, however, the $\pm 3\sigma$ interval at a value r does not contain zero, then the difference between the two PDFs cannot be explained simply by random error, and the null hypothesis is rejected. The $\pm 3\sigma$ interval shown in Fig. 3b contains zero for every value of r and, therefore, reflects that all differences between the two PDFs are attributable to random error. Defining a threshold below $\pm 3\sigma$ would lead to conclusions of structural differences between the two PDFs, as the entire range of r would not contain zero. As a result of this finding, $\pm 3\sigma$ difference plot intervals that do not include zero are assumed to be indicative of statistically significant structural dissimilarities between experimental PDFs for the remainder of this manuscript.

It is worthwhile to point out that the aforementioned conclusion concerning the $\pm 3\sigma$ threshold is not universal; rather, it is dependent on the PXRD experimental parameters. Longer irradiation times or different experimental geometries may result in better counting statistics, hypothetically producing relative initial error estimates orders of magnitude less than the ones illustrated herein. The principles surrounding error propagation and the conclusions drawn from statistical hypotheses testing outlined previously, however, are valid and warrant application when drawing inferences from differences between multiple analytical results.

From Table I, the calculated ideal T_g for a 75 wt% felodipine:PVPva amorphous molecular solid dispersion is 62°C. The experimentally determined T_g for the co-solidified product (Fig. 6), cycled through the event three times, was 67 ± 0.02°C and in good agreement with the ideal value. The ideal T_g for a 75 wt% terfenadine:PVPva (Table I) is 77°C. The experimentally determined T_g for the co-solidified product (Fig. 7), cycled through the event three times, was 60 ± 0.2°C. In both instances, a single T_g intermediate to the individual amorphous phase T_g that remains constant upon cycling was observed for the co-solidified products (Figs. 6 and 7). From purely thermal analyses, both co-solidified products may be classified as amorphous molecular solid dispersions due to the presence of only a single T_g intermediate to the pure amorphous phase T_g events.

From Fig. 4a, the scaling constant-derived concentrations of 81 wt% and 19 wt% felodipine and PVPva, respectively, (Table I) deviate substantially from the theoretical values of 75 wt% and 25 wt%. The sum-of-squares agreement factor (R) shows an error estimate of 21% between the calculated PDF and the co-solidified product PDF. From the difference plot in Fig. 4b, variations between the two patterns are observed within the range of 6–9 Å that are not explained by random error as indicated by portions of the error interval not encompassing zero (green dots). As previously suggested, this result would be indicative of a true amorphous molecular solid dispersion, as the product would have short-range order (*i.e.* nearest neighbor and next nearest neighbor interatomic distances) not explained by either pure component PDF.

From Fig. 5a, the scaling constant-derived concentrations of 73 wt% and 27 wt% drug and polymer, respectively, (Table I) are close to the theoretical values of 75 wt% drug and 25 wt% polymer. The sum-of-squares agreement factor (R) shows an error estimate of only 8% between the calculated PDF and the co-solidified product PDF (Table I). Upon inspection of the difference plot uncertainty interval in Fig. 5b, it was found that zero is contained within the $\pm 3\sigma$ interval over the entire range of r. The short-range order displayed in the PDF of the co-solidified product is well explained by that found in the individual amorphous components and thereby negates formation of a unique packing pattern. The terfenadine: PVPva dispersion product, therefore, is phase-separated.

A plausible explanation as to why a second T_g was not observed for the terfenadine co-solidified product was extrapolated from Newman *et al.* (6). Close inspection of Fig. 7 shows the T_g of the dispersion product to be nearly equal to the T_g of amorphous terfenadine. Since terfenadine represents the major phase of the dispersion (75 wt%), PVPva only constitutes 1.25 mg of a 5 mg sample. As the concentration of the PVPva amorphous domain decreases with respect to that of the amorphous terfenadine, the heat capacity change at the PVPva glass transition becomes so subtle relative to that of amorphous drug that it is not detectable using standard DSC.

CONCLUSION

The successful propagation of an initial error estimate through the PDF transform enabled statistically based conclusions to be drawn from multiple pattern comparisons. It was found that difference plots calculated from linear combinations of amorphous phase PDFs and co-solidified product PDFs could be used to differentiate between phase-separated systems and amorphous molecular solid dispersions. The calculation of error intervals on the difference plot assisted this classification scheme by providing statistical thresholds to define structural dissimilarities as opposed to subjective interpretation. Though this study does not define a universal threshold for differentiation of random errors and structural dissimilarities, the principles developed herein may be adapted and applied accordingly. Future work aims to address additional contributors to overall experimental uncertainty in an attempt to arrive at more universal criteria for defining an error threshold.

ACKNOWLEDGEMENTS

MM would like to acknowledge a pre-doctoral fellowship from the American Foundation for Pharmaceutical Education.

REFERENCES

1. Bates S, Kelly RC, Ivanisevic I, Schields P, Zografi G, Newman AW. Assessment of defects and amorphous structure produced in raffinose pentahydrate upon dehydration. J Pharm Sci. 2007;96:1418–33.
2. Atassi F, Mao C, Masadeh AS, Byrn SR. Solid-state characterization of amorphous and mesomorphous calcium ketoprofen. J Pharm Sci. 2010;99:3684–97.
3. Sheth AR, Bates S, Muller FX, Grant DJW. Local structure in amorphous phases of piroxicam from powder x-ray diffractometry. Cryst Growth Des. 2005;5:571–8.
4. Heinz A, Strachan CJ, Atassi F, Gordon KC, Rades T. Characterizing an amorphous system exhibiting trace crystallinity: a case study with saquinavir. Cryst Growth Des. 2008;8:119–27.
5. Moore MD, Steinbach AM, Buckner IS, Wildfong PLD. A structural investigation into the compaction behavior of pharmaceutical composites using powder X-ray diffraction and total scattering analysis. Pharm Res. 2009;26:2429–37.
6. Newman A, Engers D, Bates S, Ivanisevic I, Kelly RC, Zografi G. Characterization of amorphous API:Polymer mixtures using X-ray powder diffraction. J Pharm Sci. 2008;97:4840–56.
7. Nollenberger K, Gryczke A, Meier C, Dressman J, Schmidt MU, Bruhne S. Pair distribution function X-ray analysis explains dissolution characteristics of felodipine melt extrusion products. J Pharm Sci. 2009;98:1476–86.
8. Ivanisevic I, Bates S, Chen P. Novel methods for the assessment of miscibility of amorphous drug-polymer dispersions. J Pharm Sci. 2009;98:3373–86.
9. Peterson PF, Bozin ES, Proffen T, Billinge SJL. Improved measures of quality for the atomic pair distribution function. J Appl Crystallogr. 2003;36:53–64.
10. Toby BH, Billinge SJL. Determination of standard uncertainties in fits to pair distribution functions. Acta Crystallogr A. 2004;60:315–7.
11. Toby BH, Egami T. Accuracy of pair distribution function analysis applied to crystalline and non-crystalline materials. Acta Crystallogr A. 1992;48:336–46.
12. Sekiguchi K, Obi N. Studies on absorption of eutectic mixtures. I. A comparison of the behavior of eutectic mixtures of sulphathiazole and that of ordinary sulphathiazole in man. Chem Pharm Bull. 1961;9:866–72.
13. Couchman PR, Karasz FE. A classical thermodynamic discussion of the effect of composition on glass-transition temperatures. Macromolecules. 1978;11:117–9.
14. Egami T, Billinge SJL. Underneath the Bragg Peaks. Structural analysis of complex materials. Oxford: Elsevier; 2003.
15. Warren BE. X-ray diffraction. New York: Dover Publications, Inc; 1990.
16. Metropolis N, Ulam S. The Monte Carlo method. J Am Stat Assoc. 1949;44:335–41.
17. Prince E. Mathematical techniques in crystallography and materials science. New York: Springer; 2004.
18. Cullity BD, Stock SR. Elements of X-ray diffraction. Upper Saddle River: Prentice Hall; 2001.